Bone 180 (2024) 116994

Contents lists available at ScienceDirect

Bone

journal homepage: www.elsevier.com/locate/bone

Full Length Article

Cortical thickness adaptation to combined mechanical loading and parathyroid hormone treatments is site specific and synergistic in the mouse tibia model

Corey J. Miller [a], Silvia Trichilo [b], Edmund Pickering [a], Saulo Martelli [a], Enrico Dall'Ara [c], Peter Delisser [d], Lee B. Meakin [e], Peter Pivonka [a,*]

[a] Queensland University of Technology, Brisbane, Queensland, Australia
[b] University of Melbourne, Melbourne, Victoria, Australia
[c] University of Sheffield, Sheffield, United Kingdom
[d] Veterinary Specialist Services, Brisbane, Queensland, Australia
[e] University of Bristol, Bristol, United Kingdom

ARTICLE INFO

Keywords:
Intermittent PTH
Mouse tibia loading
Bone adaptation
Combined treatment
Site-specific response
Synergistic effect

ABSTRACT

In this study, we aimed to quantify the localised effects of mechanical loading (ML), low (20 μg/kg/day), moderate (40 μg/kg/day) or high (80 μg/kg/day) dosages of parathyroid hormone (PTH), and combined (PTHML) treatments on cortical bone adaptation in healthy 19-week old female C57BL/6 mice. To this end, we utilise a previously reported image analysis algorithm on μCT data of the mouse tibia published by Sugiyama et al. (2008) to measure changes in cortical area, marrow cavity area and local cortical thickness measures (ΔCt.Ar, ΔMa.Ar, ΔCt.Th respectively), evaluated at two cross-sections within the mouse tibia (proximal-middle (37 %) and middle (50 %)), and are compared to a superposed summation (P + M) of individual treatments to determine the effectiveness of combining treatments in vivo. ΔCt.Ar analysis revealed a non-linear, synergistic interactions between PTH and ML in the 37 % cross-section that saturates at higher PTH dosages, whereas the 50 % cross-section experiences an approximately linear, additive adaptation response. This coincided with an increase in ΔMa.Ar (indicating resorption of the endosteal surface), which was only counteracted by combined high dose PTH with ML in the middle cross-section. Regional analysis of ΔCt.Th changes reveal localised cortical thinning in response to low dose PTH treatment in the posteromedial region of the middle cross-section, signifying that PTH does not provide a homogeneous adaptation response around the cortical perimeter. We observe a synergistic response in the proximal-middle cross-section, with regions of compressive strain experiencing the greatest adaptation response to PTHML treatments, (peak ΔCt.Th of 189.32, 213.78 and 239.30 μm for low, moderate and high PTHML groups respectively). In contrast, PTHML treatments in the middle cross-section show a similar response to the superposed P + M group, with the exception of the combined high dose PTHML treatment which shows a synergistic interaction. These analyses suggest that, in mice, adding mechanical loading to PTH treatments leads to region specific bone responses; synergism of PTHML is only achieved in some regions experiencing high loading, while other regions respond additively to this combined treatment.

1. Introduction

Degenerative bone diseases such as osteoporosis are a leading health concern, causing increased bone fragility and high fracture risk [1,2]. Current drug treatments for osteoporosis can be divided into two categories based on their mechanism of action: (i) anti-resorptives drugs (e.g., denosumab and bisphosphonates) that significantly slow the rate of bone loss by suppressing osteoclastic activity, and (ii) anabolic drugs (e.g., teriparatide and romosozumab) that promote bone formation [3,4]. The latter drugs are used for severe osteoporosis where rapid bone formation is crucial for preventing fractures. Teriparatide, a parathyroid hormone (PTH) analogue, has been shown to induce both anabolic and catabolic bone responses on the different bone surfaces [5,6]; the major concern of intermittent delivery of PTH (iPTH) treatments is that

* Corresponding author.
E-mail address: peter.pivonka@qut.edu.au (P. Pivonka).

https://doi.org/10.1016/j.bone.2023.116994
Received 24 October 2023; Received in revised form 17 December 2023; Accepted 18 December 2023
Available online 20 December 2023

increased remodelling temporarily increases cortical bone porosity, which poses an increased fracture risk.

Alongside drug treatments, physical activity (i.e., exercise-induced mechanical loading) has been identified as a potent anabolic bone stimulus [7–10]. Bone's response to mechanical stimuli has been described using Frost's mechanostat theory [11]: consistently elevated levels of dynamic strain above a homeostatic strain threshold induces the formation of new bone, whereas decreased strain due to under-loading/disuse leads to bone resorption. However, in strength-compromised osteoporotic bones, excessive amounts of loading may increase the risk of injury or fracture. While mechanical loading has gained popularity as a physical therapy for osteoporosis intervention, the efficacy of such a treatment has been difficult to demonstrate in human studies, due to both the slow bone (re)modelling response and difficulties in patient compliance to prescribed physical exercise [12].

Combining iPTH and mechanical loading treatments has been hypothesised to enhance the anabolic bone response compared to delivering the treatments individually. Studies in healthy rats [13,14] and mice [15–18] have shown evidence of an enhanced or synergistic response to these treatments combined, both with respect to trabecular and cortical bone compartments. The study performed by Sugiyama et al. [18] investigated the treatment response to strain-matched loads across multiple PTH doses in mice, highlighting a synergistic response occurring at the maximal dosage of 80 μg/kg/day [18]. However, this study presented findings as volumetric changes; while PTH treatments are considered to be taken up homogeneously throughout the body, the adaptive response to mechanical loading is a local (i.e., site-specific) phenomenon, tied to the mechanostat and local strain environment [11,19,20]. Cortical bone measurements in PTH and combined studies are typically presented as either volumetric [16,18] or areal [21] growth. While ΔCt.Th has been measured in some combined treatment studies, these local measures are averaged over cross-sections or regions of bone and therefore hide the local effect of formation and resorption [15,17,22]. The adaptation response to mechanical loading has been measured to discrete cortical thickness changes (ΔCt.Th), highlighting that various regions around the cortical surface respond differently with respect to the loading environment [23–26]. However, it is not yet clear how the resultant adaptation due to PTH or combined PTH and mechanical loading treatments are distributed around the cortical shell. Without such a comparison, it is not possible to accurately assess and compare the trends of combined versus individual treatments, nor is it possible to accurately compare the trends of increasing dosages.

In this paper, we aim to investigate the cortical bone adaptation response to combined mechanical loading (ML) and PTH treatments at the local cortical thickness level. Using a previously developed cortical thickness measurement technique [25], we re-analyse the previously published experimental data of Sugiyama et al. [18] in order to quantify cortical thickness changes in responses to ML, PTH and combined (PTHML) treatments. Through this analysis we aim to determine: (i) how increased PTH dosages affect the cortical bone adaptation response, (ii) whether PTH leads to uniformly or non-uniformly distributed Ct.Th adaptation around the cortical shell, and (iii) whether a combined PTHML treatment provides an enhanced or synergistic effect on Ct.Th adaptation. We evaluated the cortical adaptation response at two commonly investigated cross-sectional regions of the mouse tibia (i.e., proximal-middle, middle), and compared the measurements to an untreated baseline control, thereby highlighting the effectiveness of each treatment regime.

2. Methods

The contralateral endpoint imaging data used in this study was previously reported in Sugiyama et al. [18], specifically the second iPTH/loading experiment. Here we provide a brief overview of the experimental design and μCT scanning protocol here, as well as our categorisation of data for analysis. Cortical thickness measurement techniques used in this study were previously outlined in Miller et al. [25]; a summary of the methods is presented below. For a detailed description of the experimental protocol, please refer to the original publications.

2.1. Experimental design

Female C57BL/6 mice were randomised into four groups at 13 weeks of age (experimental day 1). Mice received daily subcutaneous, intermittent treatment of either vehicle, low, medium or high doses of PTH (99.7 % saline ($n = 6$), 20 μg/kg/day (n = 6), 40 μg/kg/day ($n = 8$) and 80 μg/kg/day ($n = 5$) respectively) daily for six weeks (hereby referred to as 'vehicle', '20 μg', '40 μg' and '80 μg'). From 17 weeks of age (experimental day 29) the right tibiae of the mice were subjected to external, dynamic axial loading (40 cycles, trapezoidal wave form, 0.025 s load time, 0.05 s hold duration, 0.025 s unload time, 40 s rest interval), approximately 30–40 min post vehicle/PTH injection, three times per week (Mon, Wed and Fri) for two weeks. Peak loads used for the different drug doses were strain-matched across the PTH treatment groups to induce the same strain distribution obtained in the vehicle-treated animals, approximately 1200 με at the medial surface of the tibiae (Vehicle = 12 N, 20 μg = 13.7 N, 40 μg = 14.7 N, 80 μg = 15.8 N). The left tibiae served as an internal, unloaded control. Mice were euthanised at 19 weeks of age (experimental day 43), and both left and right tibiae were scanned using high-resolution μCT (SkyScan 1172 (SkyScan, Kontich, Belgium), pixel size 4.97 μm).

For the purposes of our study, imaging data was divided into four classifications: 1) Ultimate control (UC) - vehicle treated, non-loaded limb, 2) Mechanical loading (ML) - vehicle treated, loaded limb, 3) Parathyroid hormone (PTH) - all non-vehicle doses, non-loaded limbs and 4) Combined treatment (PTHML) - all non-vehicle doses, loaded limbs. To analyse the effects of PTHML, the mean individual treatments of PTH and ML were added together to create the P + M group, representing the case of additive cortical bone adaptation.

2.2. Image pre-processing

Tibial μCT image stacks were normalised along their proximal-distal direction (i.e., z-axis), with cross-sections taken from the proximal-middle (z = 37 %) and middle (z = 50 %) portions of the tibia (see Fig. 1A). As per our previous study, a single cross-sectional image was used for analysis Miller et al. [25]. μCT images were grouped based on drug treatment dosage, z location and non-loaded/loaded limb. All images from the right limb were flipped about the sagittal plane to match the orientation of the left limb for comparison.

Images were analysed using a customised algorithm developed in MATLAB 2021b. Images were first binarised using Otsu thresholding, and imperfections (i.e., pores/holes) were filled. Note that filling of pores within images does not significantly affect our results. It simply removes errors in calculating cortical thickness. While filling pores does shift the centroid slightly, the direction to the fibula centroid is not affected due to the distance between the two centroids. Woven bone was highly prevalent throughout limbs that had received high PTH or combined PTHML treatments; additional filters were applied to fill the gaps while persevering the external perimeters of the cortical shell to enable the measurement of cortical thickness. Pixels around the periosteal and endosteal surfaces were extracted and mapped into individual arrays of (x,y) coordinates. Periosteal position (P^P) distributions were aligned to a characteristic point on the periosteum ($P^P = 0$), highlighted in Fig. 1B-C; the characteristic point was defined by connecting the centroids of the tibia and fibula, and selecting the intersection point of this line and the periosteal surface of the tibia. Following a clockwise direction from the characteristic point, pixels around the periosteal surface were normalised between 0 and 1, allowing accurate and consistent comparisons between tibiae within each treatment group.

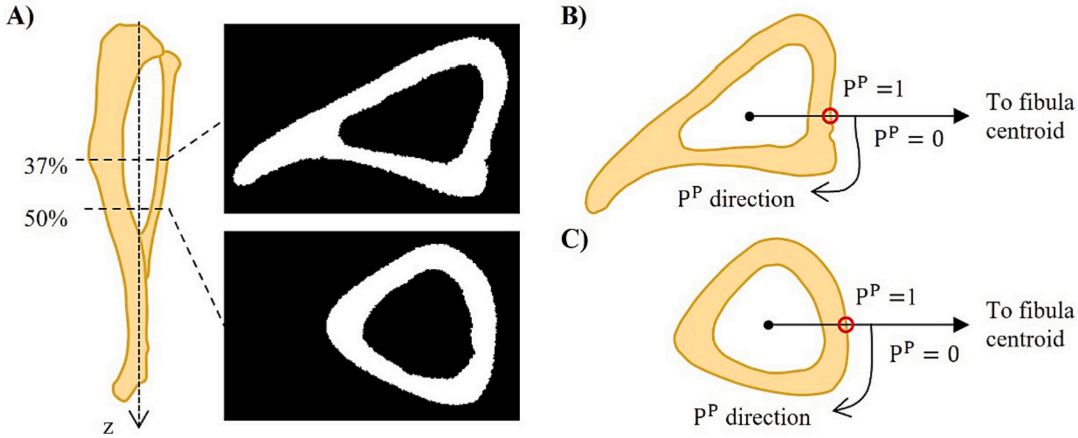

Fig. 1. Image Pre-Processing. A) Longitudinal location of slices, showing binarised and filled slices. B, C) Alignment of the periosteal boundary P^P to a characteristic point defined as the intersection of the tibial periosteum and the tibia-fibula centroid line.

2.3. Beam theory analysis of the Tibia

A mechanical analysis was performed at both tibial cross-sections to link strain patterns to thickness changes. Strains throughout the cortical shell were calculated using Euler-Bernoulli beam theory which has been shown to be an effective method for calculating axial strains in the tibia [27–32]. Representative strain values were calculated on a sample tibia from the UC group ($F = 12$ N). Our intention was not to provide a direct link between strain magnitudes and the adaptive response, rather the analysis highlights regions of the cross-sections experiencing tensile and compressive strains and regions of peak strain magnitude.

Beam-theory analysis was performed in accordance with [31,33]. In summary, the axial compressive load F was assumed to act purely axially, concentrated at a point between the tibial condyles at the tibial plateau, with the location projected onto the cross-section analysed (z). The load F induces a normal force N and bending *moments* $M_x = N \cdot d_y$ and $M_y = N \cdot d_x$ in the cross-section, where d_x and d_y represent the distance between the load location and cross-sectional centroid. Internal strains within the cross-section can be calculated using the following equation:

$$\varepsilon\left(P^P(x,y)\right) = \frac{1}{E}\sigma\left(P^P(x,y)\right) = \frac{1}{E}\left(\frac{N}{A} + \left(\frac{M_x I_{yy} + M_y I_{xy}}{I_{xx}I_{yy} - I_{xy}^2}\right)\cdot y - \left(\frac{M_y I_{xx} + M_x I_{xy}}{I_{xx}I_{yy} - I_{xy}^2}\right)\cdot x\right)$$

where E is the Young's Modulus (14.8 GPa, Kohles et al. [34]), A is the cross-sectional area, I_{xx}, and I_{yy} are the second moments of area with respect to the x − and y − axis respectively, and I_{xy} is the product moment of area. Second moments of area were calculated using the parallel axis theorem on the binarised images, treating each white pixel (i.e., bone) as a square of area = 24.70 μm^2. We note that strain calculations were performed prior to the filling of pores detailed in the previous section, and as such the centroids and second moments of area are not affected due to pre-processing.

To aid with interpretation and discussion of our results, four strain regions were highlighted: posterior ($P^P = 0.05$), anterior ($P^P = 0.50$), lateral ($P^P = 0.30$), and medial ($P^P(z = 37\ \%) = 0.85$, $P^P(z = 50\ \%) = 0.67$). These locations align with regions of maximal tension/compression (anterior/posterior), and regions of very low strain i.e., the neutral bending axis (medial and lateral).

2.4. Cortical analysis

Cortical bone adaptation was measured with respect to Cortical Area (Ct.Ar), Marrow Cavity Area (Ma.Ar) and Cortical Thickness (Ct.Th). Area values were calculated from the cross-sectional images by summing the total number of respective pixels (i.e., cortex or internal cavity) and multiplying by the pixel area resolution (i.e., 24.70 μm^2); we note that this step was completed prior to the filling of woven bone pores.

Cortical thickness was calculated using our previously reported hybrid measurement technique [25]. Two types of thickness measurements were used (shown in Fig. 2): i) minimum distance between a given periosteal pixel and the nearest endosteal pixel (Fig. 2A), and ii) perpendicular distance between a given periosteal pixel and the next cortical intersection, periosteal or endosteal (Fig. 2B). Both techniques were calculated for all points around the periosteal surface, with the smaller of the two selected as the representative local cortical thickness measure at each point. The resultant thickness distribution profile was filtered using a lowpass Butterworth filter (zero phase shift, 2nd order, 0.4 Nyquist cutoff rate) to remove high-frequency noise.

To account for the difference in length of cortical perimeters due to variability between animals and the adaptation process, thickness distributions were re-sampled to a total of $n = 750$ periosteal points. Furthermore, to ensure that the same cortical regions were compared, additional alignment was required. For the z = 50 % cross-section, where the cross-section remained approximately circular, thickness distributions were linearly interpolated and aligned through cross-covariance with respect to the UC. For the z = 37 % section, where adaptation along the tibial ridge significantly affected the alignment of P^P points between all treatment combinations, four common peaks/troughs were located in the Ct.Th distribution that represented key bony features (e.g., tip of the tibial ridge) were located, and measurements were consistently realigned across all tibiae. Net adaptation due to a given treatment T (ML, PTH, PTHML) was measured with respect to the UC group at all cortical points P^P. Area and thickness changes (ΔCt.Ar, ΔMa.Ar, ΔCt.Th) can therefore be calculated as:

$$\Delta Ct.Ar_T = Ct.Ar_T - Ct.Ar_{UC}$$

$$\Delta Ma.Ar_T = Ma.Ar_t - Ma.Ar_{UC}$$

$$\Delta Ct.Th_T\left(P^P\right) = Ct.Th_{T\left(P^P\right)} - Ct.Th_{UC}\left(P^P\right)$$

2.5. Statistical analysis

One- and two-way ANOVA were performed on Ct.Ar and Ma.Ar measurements to determine the significance of ML and PTH on adaptation as either separate or combined treatments. For Ct.Th measurements, this was expanded to a three-way ANOVA by considering periosteal position (i.e., P^P) as a third independent variable. Mean values (ΔCt.Ar, ΔMa.Ar, ΔCt.Th) and standard deviation were calculated

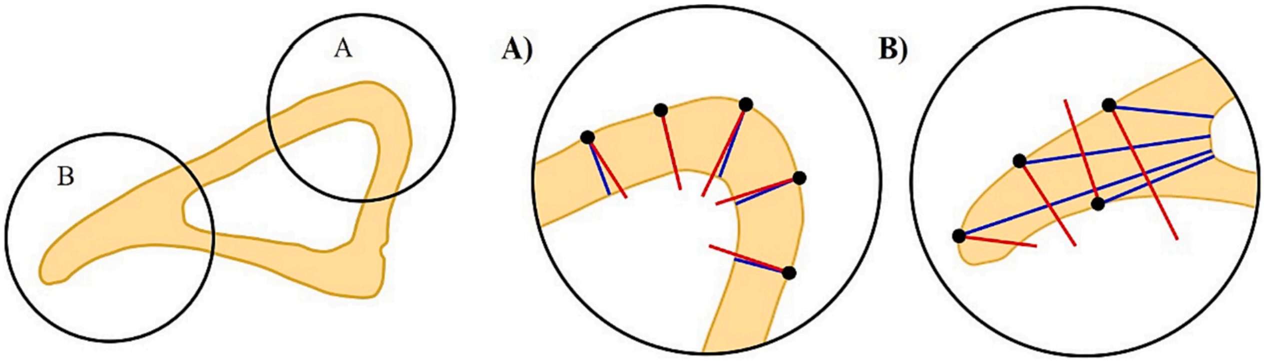

Fig. 2. Hybrid measurement technique in the z = 37 % section, highlighting two measurement cases. A) Case 1: thickness measurements in the postero-medial region of the cross-section minimum distance (blue) and perpendicular distance (red) measurements are similar, with minimum distance providing shorter measurements. B) Case 2: thickness measurements along the tibial ridge. The two measurement techniques show major differences, with perpendicular distance providing the shorter measurement. (For interpretation of the references to colour in this figure legend, the reader is referred to the web version of this article.)

across all specimens within a given dosage-loading-location group at each point P^P. For simplicity of notation, all subsequent presentations of ΔCt.Ar, ΔMa.Ar, ΔCt.Th will refer to the mean values. Areal and thickness measurements were evaluated through a two-sample *t*-test for each treatment per tibial cross-section, comparing the observed adaptation to the UC (i.e., unadapted state); at the Ct.Th level, this was evaluated at all points P^P. For this study, a *p*-value <0.05 represents statistical significance for both ANOVA and two-sample *t*-tests. We note that as the P + M group was calculated through the summation of two mean datasets, statistical significance was not calculated.

3. Results

3.1. Mechanical strain analysis

Shown in Fig. 3, strains in the posterior region (−6406 με, −7050 με for 37 % and 50 % respectively) were observed to experience a higher strain magnitude compared to the anterior regions (4088 με, 6488 με for the 37 % and 50 % respectively). Both the lateral and medial regions were observed to experience very low levels of strains, being closely located near the neutral bending axis.

3.2. Statistical significance

Shown in Table 1, Ct.Ar changes were observed to be statistically significant for all treatments and dosage levels in both the 37 % and 50 % cross-sections. Ma.Ar were found to be statistically significant under PTH-only treatments, with the exception of 80 μg in the 50 % cross-section ($p = 0.890$), and in the case of combined 40 μg and ML treatment in the 37 % section ($p = 0.039$); all remaining treatments were not found to induce statistically significant changes to Ma.Ar.

Table 1
Statistical significance of ΔCt.Ar and ΔMa.Ar at the z = 37 % and z = 50 % cross-sections, determined through two-sample t-test (* indicates $p < 0.05$ statistical significance).

	ΔCt.Ar		*ΔMa.Ar*	
	37 %	50 %	37 %	50 %
ML				
12 N	0.001*	<0.001*	0.080	0.682
PTH				
20 μg	<0.001*	0.001*	0.003*	0.042*
40 μg	<0.001*	<0.001*	0.006*	<0.001*
80 μg	0.001*	0.001*	0.001*	0.890
PTHML				
20 μg	<0.001*	<0.001*	0.249	0.751
40 μg	<0.001*	<0.001*	0.039*	0.068
80 μg	<0.001*	<0.001*	0.083	0.170

Table 2 shows the results of one- and two-way ANOVA performed on Ct.Ar and Ma.Ar results. One-way ANOVA shows that both ML and PTH treatments individually provide a statistically significant adaptation response in the observed Ct.Ar and Ma.Ar measurements. The two-way interaction between treatments was shown to be statistically significant in the 37 % cross-section for Ct.Ar and Ma.Ar. However, the interaction did not show significance at the 50 % cross-section for either area measurement.

ANOVA of the Ct.Th measurements resulted in *p*-values below 0.05 for treatments and periosteal position for all individual (one-way), paired (two-way) and set of three (three-way) tests at both the z = 37 %

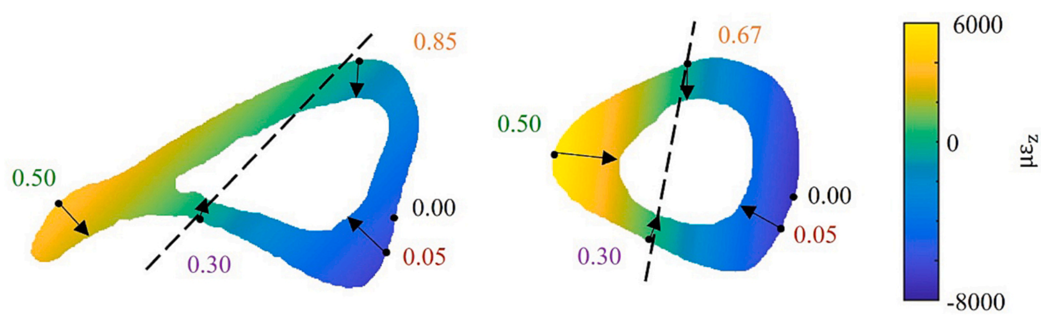

Fig. 3. Longitudinal strain calculated for the 37 % and 50 % cross-sections, calculated on a sample tibia from the UC group (F = 12 N). Four regions of interest are identified: posterior ($P^P = 0.05$), lateral ($P^P = 0.30$), anterior ($P^P = 0.50$), and medial ($P^P(z = 37\ \%) = 0.85$ $P^P(z = 50\ \%) = 0.67$). Arrows indicate the direction of cortical thickness measurement.

Table 2
One- and two- way ANOVA results for Ct.Ar and Ma.Ar measurements (* indicates $p < 0.05$ statistical significance).

	Ct.Ar		Ma.Ar	
	37 % *p*-value	50 % *p*-value	37 % *p*-value	50 % *p*-value
One-way ANOVA				
ML	<0.001*	<0.001*	0.041*	0.004*
PTH	<0.001*	<0.001*	0.013*	<0.001*
Two-way ANOVA				
ML x PTH	0.010*	0.835	0.035*	0.506

and z = 50 % cross-sections.

3.3. Cortical area adaptation

Fig. 4 shows the ΔCt.Ar and ΔMa.Ar results for both the z = 37 % and z = 50 % cross-sections. Increased PTH dosages (blue line) provided a non-linear response in the z = 37 % cross-section, and a pseudo-linear response in the z = 50 % cross-section, with these trends becoming enhanced with the inclusion of mechanical loading (orange line). Comparing the changes of ΔCt.Ar for the combined treatment (i.e., PTHML) response to the added P + M group (dashed black line), the z = 37 % exceeds the summative values whereas the z = 50 % is equivalent. Across all treatments, increases of Ct.Ar were more prominent in the 37 % cross-section compared to the 50 % cross-section.

Positive values observed in ΔMa.Ar measurements indicate a net loss of bone on the endosteal envelope of the cortical shell. The z = 37 % cross-section experienced an expansion of the marrow cavity across all PTH dosage (ΔMa.Ar ≈ 0.072 mm2). While the 50 % cross-section shows resorption at 20 μg and 40 μg doses of PTH, supplying a dose of 80 μg was sufficient to elicit zero net change in Ma.Ar. In both sections, application of mechanical loading alongside PTH mitigated some of the endosteal resorption, but only showed net formation under the combined ML and 80 μg PTH treatment regime. The combined PTHML treatment did not show any enhanced benefits over the P + M group in the 37 % cross-section, but exceeded the P + M results in the 50 % cross-section.

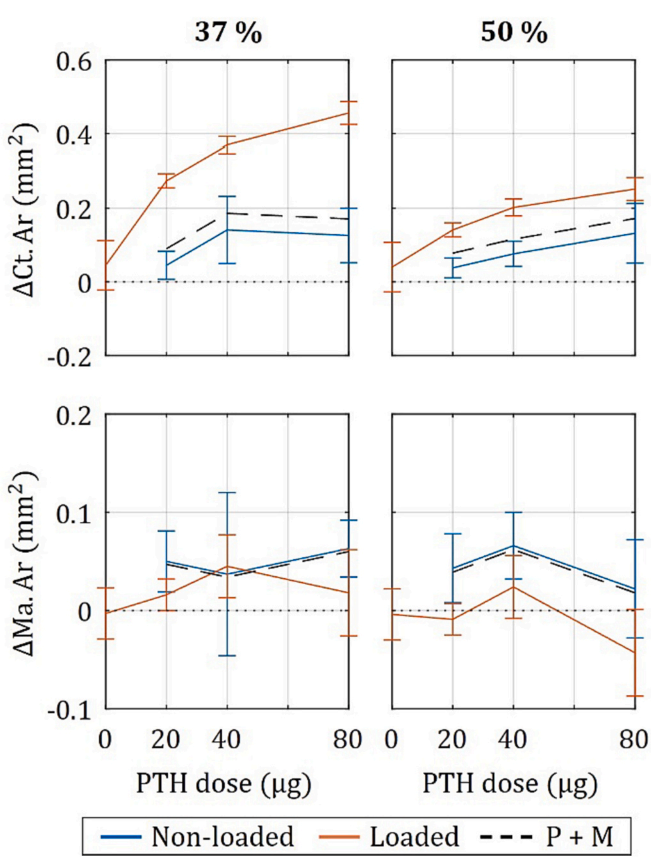

Fig. 4. Mean ΔCt.Ar changes at the z = 37 % and z = 50 % cross-sections. Blue lines = no applied load (i.e., left limb), orange line = load applied (i.e., right limb). Dashed black = P + M. (For interpretation of the references to colour in this figure legend, the reader is referred to the web version of this article.)

3.4. Cortical thickness adaptation

Throughout the remainder of this analysis, reference made to the four strain regions will refer to approximately $P^P \pm 0.15$ of the previously mentioned anterior, posterior, lateral and medial positions. Fig. 5A-C shows the ΔCt.Th results for the 37 % cross-section, with results grouped by PTH dosage. The ML group (blue line) showed a two peak formation response in the anterior and posterior regions of the cross-section ($\Delta Ct.Th_{ML}$ = 37.65 μm and 92.21 μm respectively), and near-zero change around the medial and lateral regions of the tibia. Anabolic benefits observed in the PTH group (orange line) were more pronounced on the anterior region of the bone ($\Delta Ct.Th_{PTH}$ = 59.64 μm, 79.84 μm and 66.82 μm for 20 μg, 40 μg and 80 μg) compared to the posterior ($\Delta Ct.Th_{PTH}$ = 26.94 μm, 54.80 μm and 46.94 μm for 20 μg, 40 μg and 80 μg). Moderate and high dose PTH treatments elicited a net formation response in the lateral region of bone ($\Delta Ct.Th_{PTH}$ = 19.42 μm and 25.27 μm for 40 μg and 80 μg), however the medial region remained approximately equal to the UC. The PTHML group (purple line) showed a greater increase in ΔCt.Th than either the ML or PTH groups alone, with the exception of the medial region under a 40 μg dosage regime. Across the three dosages, peak formation amounts were greatest in the posterior region of the bone and increased with PTH dosage ($\Delta Ct.Th_{PTHML}$ = 189.32 μm, 213.78 μm and 239.30 μm for the 20 μg, 40 μg and 80 μg doses respectively). A second peak was identified in the anterior region of the cross-section ($\Delta Ct.Th_{PTHML}$ = 139.66 μm, 183.82 μm and 139.31 μm for the 20 μg, 40 μg and 80 μg doses respectively). Similar to PTH alone, the PTHML group showed a net formation response at the lateral region, with a near zero change on the medial. The changes in Ct.Th for the in silico P + M group (dashed black line) were generally smaller than the PTHML group, with the exception of regions near the null axis.

Results observed in the 50 % cross-section (Fig. 5E-G) show a reduced ΔCt.Th magnitude and a smoother curve along the periosteum compared to the 37 % cross-section. The ML group (blue line) showed a peak anterior and posterior formation of 53.10 and 56.59 μm respectively, with zero change at the medial and lateral regions. The PTH group (orange line) presented a more uniform response with no discernible peaks, with the exception of the posterior region of the cross-section ($0.75 < P^P \leq 1.0$); here, low dose PTH treatment presented a net loss of Ct.Th ($\Delta Ct.Th_{PTH}$ = −18.76 μm), moderate dose PTH provided approximately zero change, while high dose PTH resulted in a net anabolic benefit exceeding mechanical loading ($\Delta Ct.Th_{PTH}$ = 68.41 μm). In contrast to the 37 % cross-section, the combined PTHML treatment exceeded the in silico P + M group only for the maximum 80 μg PTH dose; for the lower PTH doses, the PTHML and P + M groups showed similar responses. Here, the anterior and posterior peaks were approximately equal to one another, increasing in magnitude with respect to the increased PTH dosages (peak $\Delta Ct.Th_{PTH}$ = 75.84 μm, 99.39 μm and 124.23 μm for 20 μg, 40 μg and 80 μg). For low and moderate PTH dosages, the PTHML group was near equivalent to the summative P + M group (dashed black line); whereas the maximal PTHML treatment exceeded the P + M group in the posterior ($0.0 < P^P < 0.25$) and anterior ($0.3 < P^P < 0.7$) regions of the cross-section.

To provide further insight into the ΔCt.Th response under different treatment regimens, Fig. 6 highlights the data from each of the four identified regions (i.e., P^P = 0.05, 0.30, 0.50, 0.67/0.85) for both the 37

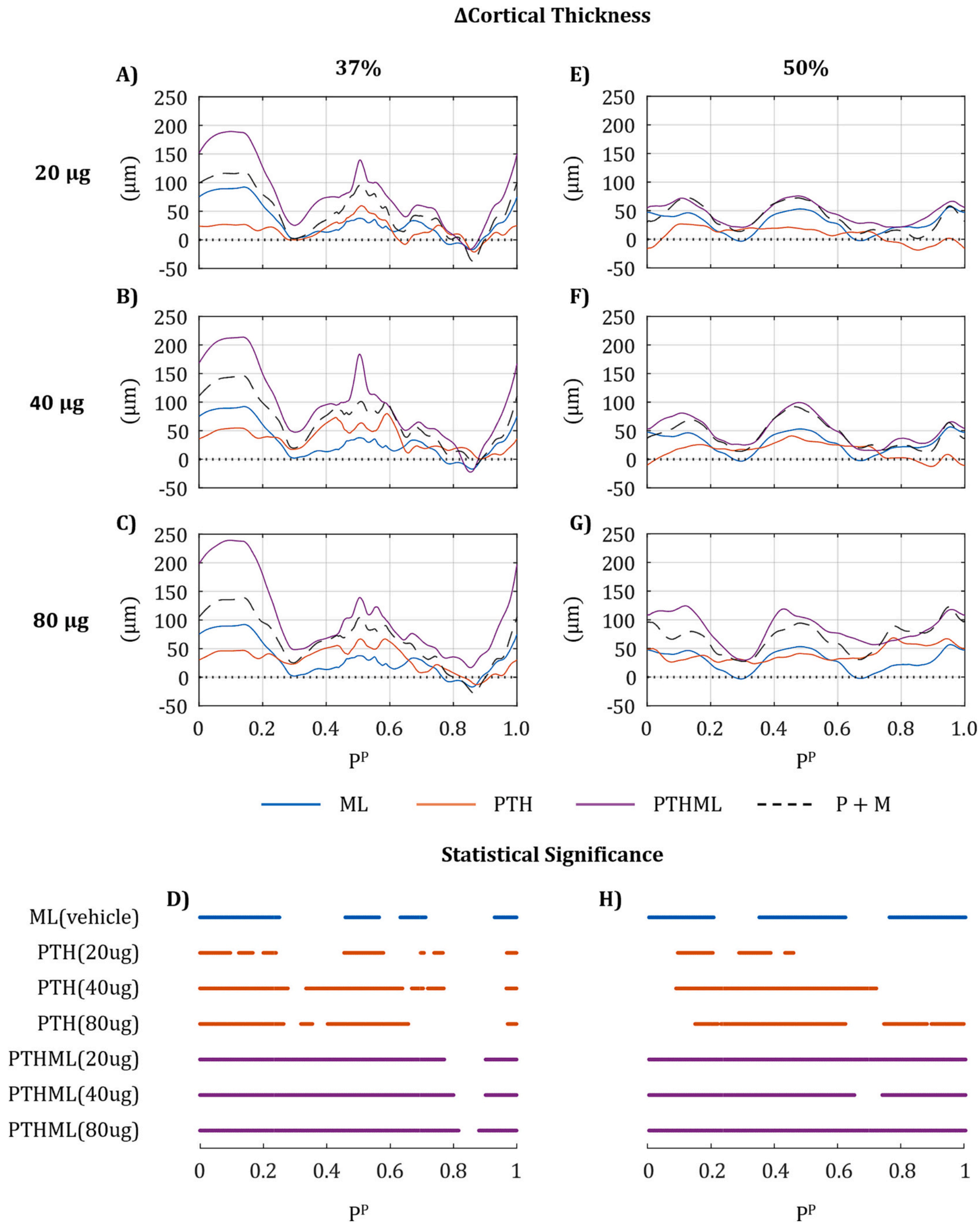

Fig. 5. Mean cortical thickness (Ct.Th) measurements around the periosteal perimeter at: A-C) 37 % cross-section, and *E*-G) 50 % cross-section, grouped by PTH dosage. Blue line = ML group (vehicle), orange line = PTH group (no load), purple line = PTHML, dashed black line = P + M superposed response. Locations around the periosteal perimeter that show statistically significant adaptation (i.e., *p*-value <0.05) are represented in D) and H) for the 37 % and 50 % cross-sections respectively. (For interpretation of the references to colour in this figure legend, the reader is referred to the web version of this article.)

% and 50 % cross-sections. In the 37 % section, for PTH treatment alone (i.e., no mechanical loading applied), the four regions each show a near constant ΔCt.Th with respect to increased dosage levels, with the anterior/posterior (red/green) regions showing a greater response compared to the lateral/medial purple/orange) regions. When loading is applied either alone or with PTH treatment, ΔCt.Th in the anterior/posterior region exhibit a nonlinear response with respect to increased PTH dosages. The addition of PTH increases ΔCt.Th in the lateral/medial regions compared to ML treatment alone, however the change shows similar trends regardless of the dose of PTH applied. In the 50 % cross-section, the response to PTH alone results in a near-consistent ΔCt.Th across all dosages in the lateral and anterior regions of the bone, whereas the medial and posterior sections show an increased response when treated with high-dose PTH. With the addition of loading, the anterior and posterior sections show a pseudo-linear increase with respect to increased PTH dosages. Similarly to the proximal-middle cross-section, the addition of PTH to ML provides an increased ΔCt.Th in the lateral/medial regions, but remains constant with increased dosages, with the exception of an enhanced response on the medial edge at the maximal 80 μg dosage.

4. Discussion

Our study investigated the effects of PTH and ML, both as individual

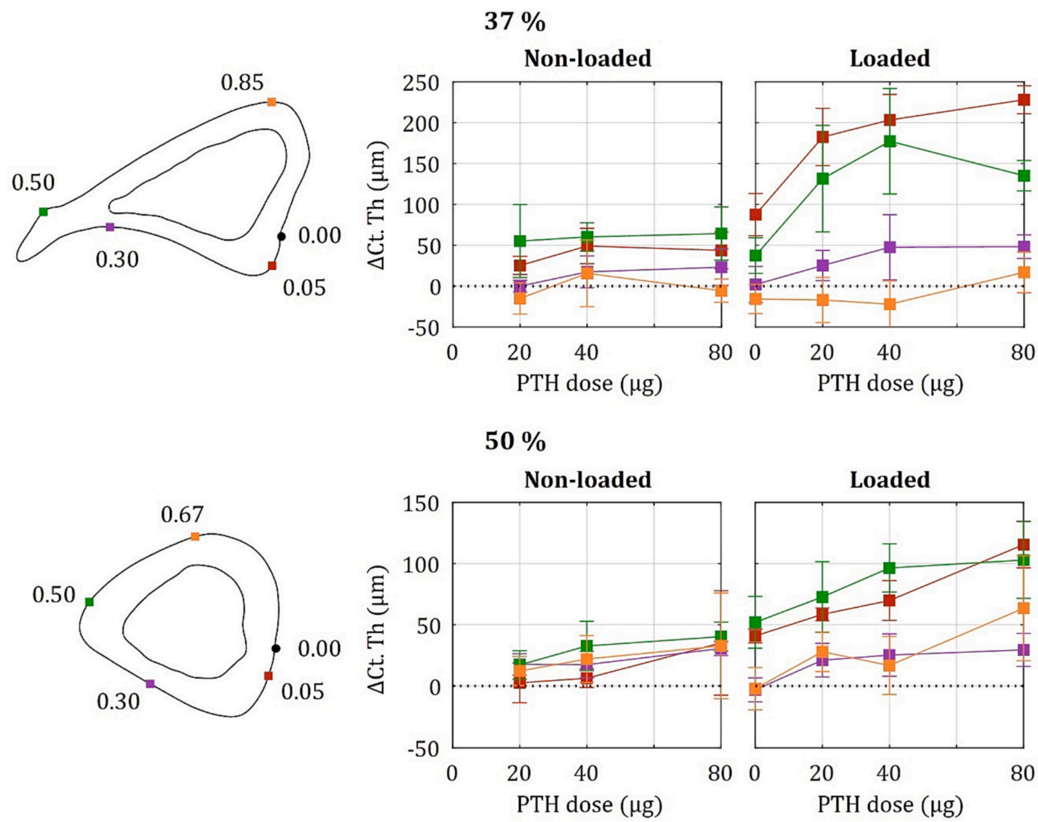

Fig. 6. Mean ΔCt.Th and standard deviation measurements at the 37 % (top) and 50 % (bottom) cross-sections, evaluated at regions of: peak tension ($P^P = 0.50$, green), peak compression ($P^P = 0.05$, red), and the neutral axis ($P^P = 0.30$, green, and $P^P = 0.85/0.67$, orange). (For interpretation of the references to colour in this figure legend, the reader is referred to the web version of this article.)

and combined treatments, and the resulting adaptation at the Ct.Ar and Ct.Th levels. Through comparison to an untreated, ultimate control, we identified that trends of the adaptation response differ between the two treatment options. Additionally, we have shown that combining the two treatment methods provides a cross-section and dose-specific synergistic effect when compared to the addition of individual treatments. This synergism is a localised phenomenon, showing the greatest response in the posterior region of the proximal-middle cross-section.

PTH's effect on cortical bone modelling varies with respect to the cortical surface. While formative trends were observed in total cortical bone area, increases to the medullary cavity show that the endosteal surface is resorbing. On the endosteal surface, PTH interacts with several stages of the remodelling cycle, inducing both catabolic and anabolic actions simultaneously [35–37]. Additionally, lining cells along the periosteum provide an additional source of anabolism unique to this surface [38,39]. This indicates that while PTH treatment shows a net anabolic benefit for cortical bone (Fig. 4), bone loss in the marrow cavity reduces some of the benefits of the treatment. This effect is partially mitigated in the 50 % cross-section, but only at a maximal dosage of 80 μg, suggesting that high doses of PTH may be required for anabolic (re) modelling to outweigh catabolic (re)modelling on the endosteal surface. Incorporation of mechanical loading with PTH clearly showed a synergistic benefit, both with respect to the cortical and medullary cavity areas, with combined PTHML treatments exceeding the sum of individual treatments. For Ct.Ar changes, this benefit followed a non-linear curve, showing that increased dosage did not provide benefits as strongly as through the initial inclusion of the two treatments. Combined treatments were also capable of overcoming the bone lost to PTH in the middle cross-section, with the 80 μg PTHML far outweighing the benefits of mechanical loading alone.

Cortical thickness changes in response to combined treatments were non-uniform and region specific. ML treatment generates formation consistent with areas of high and low strain, similar to previous findings [25]. PTH treatments alone were shown to provide a more evenly distributed anabolic response; however, this response was less prominent in the posteromedial regions of the two cross-sections analysed (i.e., $0.0 \le P^P < 0.3$, $0.8 < P^P \le 1.0$), with cortical thinning present at low and moderate dose PTH in the middle cross-section. This indicates that, while PTH is capable of increasing cortical area, this is not uniform and may have detrimental effects in certain regions of the bone. Combined PTHML treatments show cross-section specific enhancements; in the 37 % cross-section, the combined treatment resulted in a synergistic response across all PTH dosages, whereas in the 50 % cross-section, only the maximal 80 μg dose was capable of providing synergy. However, we note that the synergistic adaptation response is far more prominent in the proximal-middle cross-section compared to the middle cross-section, even though strains were higher in the latter section. This implies that the synergistic response within the cortical bone tissue is not tied to a strain magnitude, and may instead be linked with alternate factors such as biological composition of the tissue; we note that histomorphometry was not included within the original study, and therefore making such correlations are outside of the scope of the present study. Considering ΔCt.Th measurements alongside ΔCt.Ar and ΔMa.Ar highlights that while PTH can provide a synergistic response with ML, the synergism is region specific with respect to longitudinal cross-section, surface and longitudinal strain directionality (i.e., compression vs tension).

The compressive region becomes highly sensitised and generates the greatest amount of synergistic bone formation in the proximal-middle section. This aligns with findings from a combined treatment study conducted by Rooney et al. [17]; however, their study found the elevated compressive response to occur in the tibial mid-diaphysis, equating to the middle section of the tibia analysed here, whereas we found an equivalent response between tensile and compressive regions (see Fig. 6). We note that the study of Rooney et al. [17] investigated a lower compressive axial load (PTH: 40 μg/kg, ML: 10.6 N). Following the findings of a recent mechanical loading study in the mouse tibia conducted by Miller et al. [40], the compressive region experiences mechano-sensitisation earlier than the tensile region, and saturation of the adaptation response begins to occur at loads of approximately 10 N. Given that the present study considered a compressive load of 14.7 N for a PTH treatment dose of 40 μg, the adaptation response in the compressive region has likely reached saturation whereas the tensile region had not, leading to the equivalent response observed between the two regions.

The synergistic response observed in our study is an agreement with the previously presented notion that PTH alters mechanical sensitivity of cells [13,18,41]. Our analysis shows that the sensitivity does not increase linearly with respect to PTH dosage levels, suggesting that there may be a saturation effect. However, this response is non-uniform, and may depend on several factors such as regional-dependent cellular concentrations. In addition to this, the response is not equivalent between longitudinal regions of the tibia; maximal Ct.Ar/Ct.Th changes occur in the proximal-middle cross-section, whereas the middle cross-section showed a reduced endosteal resorption response (i.e., ΔMa.Ar). Suggested by Skerry, bone may consist of multiple mechanostats that are region-specific [42,43], with recent findings suggesting that formation thresholds can vary amongst longitudinal location and strain region [44]; the findings of Miller et al. [25,40] provide quantitative evidence that this may be the case with respect to increased mechanical loading. It stands to reason that the different synergistic response rates to PTHML within different regions is due to interactions with multiple mechanostats, however no such connection has been confirmed.

One limitation of the study is the presence of woven bone formation. Woven bone occurs in response to rapid growth, and often occurs in response to fracture healing [45,46]. While we observed significant areal and thickness changes, the resultant woven bone is mechanically weaker compared to lamellar bone and does not represent a healthy adaptation response. In a study investigating treatments of similar magnitude in ovariectomised mice (12 N peak load, 100 μg/kg/day) [22,23], woven bone formation was not present. We also acknowledge that the data used in the present study [18] was performed on healthy mice and used strain-matched loads, with high-dose PTH mice receiving higher peak load magnitudes (i.e., treatments of 80 μg PTH received 15.8 N external axial load). Additionally, mice in the present study received four weeks of PTH pre-treatment before the mouse underwent external loading; the additional PTH pre-treatment is likely responsible for the synergistic adaptation response. To maximise our understanding of the adaptive response, further studies in OVX mice should be performed with PTH pre-treatment to consider how this would affect cortical bone adaptation in a disease state model.

Due to the woven bone, performing a full mechanical analysis was also beyond the scope of this study. The local strain environment plays a significant, region-specific role in cortical bone adaptation [40]. However, as mentioned above, the formation of woven bone directly impacts the mechanical properties of bone and represents an unhealthy adaptation response [45,46]. Given that the formation of woven bone was not present in all datasets, correlating the local strain magnitude to the measured adaptation response would not provide an accurate representation of the mechanical-based adaptation observed. While tracking sclerostin expression has been performed in other studies to connect mechanical and biological interactions [47–49], such investigation was not conducted in the original study of Sugiyama et al. [18]. In future studies, investigating the expression of sclerostin in response to combined mechanical loading and PTH treatments would serve to further expand upon the results presented here.

Finally, the data set we investigated only considered a single strain-matched peak load case. Mechanical loading has been shown to exhibit a pseudo-linear adaptive response to increasing peak load magnitude [25,50]. In contrast, the present study has shown that adaptation to PTH exhibits pseudo-linearity with respect to dosage, but only when considering either ΔCt.Ar or the tensile region of the cross-section. As only one strain matched load condition was considered here, we can not be certain what trends would be observed from lower peak load values combined with the same PTH doses. To fully understand the synergistic response, further study would need to be conducted on intermediate loading cases.

5. Conclusion

In this paper, we used a previously developed measurement technique to analyse the effects of mechanical loading, PTH, and combined treatments at the cortical area and cortical thickness levels. We establish a statistically significant, synergistic effect of combined treatment methodologies in the proximal-middle section of the tibia; however, the middle section only shows synergy at the maximal PTH dose of 80 μg/kg/day, with lower doses providing only an additive adaptive benefit. Understanding the interaction between PTH and mechanical loading is highly beneficial in the context of designing targeted, subject-specific treatments to provide additional bone formation in critical (e.g., highly porous) regions. Additionally, this knowledge will be helpful in guiding the creation of in silico tools to investigate cortical bone adaptation to combined treatments, which is the scope of a future study.

CRediT authorship contribution statement

Corey J. Miller: Writing – review & editing, Writing – original draft, Visualization, Validation, Methodology, Investigation, Formal analysis, Data curation, Conceptualization. **Silvia Trichilo:** Writing – review & editing, Methodology, Formal analysis, Conceptualization. **Edmund Pickering:** Writing – review & editing, Supervision, Methodology, Formal analysis, Conceptualization. **Saulo Martelli:** Writing – review & editing, Methodology, Formal analysis. **Enrico Dall'Ara:** Writing – review & editing, Supervision, Investigation. **Peter Delisser:** Writing – review & editing, Data curation. **Lee B. Meakin:** Writing – review & editing, Data curation. **Peter Pivonka:** Writing – review & editing, Supervision, Project administration, Formal analysis, Data curation, Conceptualization.

Funding

Mr. Miller acknowledges the support of an APA scholarship by Queensland University of Technology. Prof. Pivonka gratefully acknowledges support from the Australian Research Council (IC190100020, DP230101404).

Availability of Data and Materials

Requests to access the datasets of this study should be directed to PP (peter.pivonka@qut.edu.au).

Declaration of competing interest

The authors hereby declare that they have no conflict of interest in the submitted manuscript.

Data availability

Data will be made available on request.

References

[1] G. Adami, A. Fassio, D. Gatti, O. Viapiana, C. Benini, M.I. Danila, K.G. Saag, M. Rossini, Osteoporosis in 10 years time: a glimpse into the future of osteoporosis, Therap. Adv. Musculoskel. Dis. 14 (2022), 1759720X221083541.

[2] D.M. Black, C.J. Rosen, Postmenopausal osteoporosis, N. Engl. J. Med. 374 (2016) 254–262.
[3] J. Barnsley, G. Buckland, P. Chan, A. Ong, A. Ramos, M. Baxter, F. Laskou, E. Dennison, C. Cooper, H.P. Patel, Pathophysiology and treatment of osteoporosis: challenges for clinical practice in older people, Aging Clin. Exp. Res. 33 (2021) 759–773.
[4] S.S. Li, S.H. He, P.Y. Xie, W. Li, X.X. Zhang, T.F. Li, D.F. Li, Recent progresses in the treatment of osteoporosis, Front. Pharmacol. 12 (2021).
[5] M. McClung, Cancel the denosumab holiday, Osteoporos. Int. 27 (2016) 1677–1682.
[6] S. Minisola, C. Cipriani, G.D. Grotta, L. Colangelo, M. Occhiuto, P. Biondi, C. Sonato, E. Vigna, M. Cilli, J. Pepe, Update on the safety and efficacy of teriparatide in the treatment of osteoporosis, Therap. Adv. Musculoskel. Dis. 11 (2019), 1759720X19877994.
[7] B.R. Beck, R.M. Daly, M.A.F. Singh, D.R. Taaffe, Exercise and sports science Australia (essa) position statement on exercise prescription for the prevention and management of osteoporosis, J. Sci. Med. Sport 20 (2017) 438–445.
[8] D. Bliuc, N.D. Nguyen, T.V. Nguyen, J.A. Eisman, J.R. Center, Compound risk of high mortality following osteoporotic fracture and refracture in elderly women and men, J. Bone Miner. Res. 28 (2013) 2317–2324.
[9] P. Ebeling, R. Daly, D. Kerr, M. Kimlin, An evidence-informed strategy to prevent osteoporosis in Australia, Med. J. Aust. 2 (2013) 90–91.
[10] S. Zhang, X. Huang, X. Zhao, B. Li, Y. Cai, X. Liang, Q. Wan, Effect of exercise on bone mineral density among patients with osteoporosis and osteopenia: a systematic review and network meta-analysis, J. Clin. Nurs. 31 (2022) 2100–2111.
[11] H.M. Frost, Bone "mass" and the "mechanostat": a proposal, Anat. Rec. 219 (1987) 1–9.
[12] S. Martelli, B. Beck, D. Saxby, D. Lloyd, P. Pivonka, M. Taylor, Modelling human locomotion to inform exercise prescription for osteoporosis, Curr. Osteoporos. Rep. 18 (2020) 301–311.
[13] H. Hagino, T. Okano, M.P. Akhter, M. Enokida, R. Teshima, Effect of parathyroid hormone on cortical bone response to in vivo external loading of the rat tibia, J. Bone Miner. Metab. 19 (2001) 244.
[14] J. Li, R.L. Duncan, D.B. Burr, V.H. Gattone, C.H. Turner, Parathyroid hormone enhances mechanically induced bone formation, possibly involving l-type voltage-sensitive calcium channels, Endocrinology 144 (2003) 1226–1233.
[15] J.D. Gardinier, F. Mohamed, D.H. Kohn, Pth signaling during exercise contributes to bone adaptation, J. Bone Miner. Res. 30 (2015) 1053–1063.
[16] S.T. Robinson, P.T. Shyu, X.E. Guo, Mechanical loading and parathyroid hormone effects and synergism in bone vary by site and modeling/ remodeling regime, Bone 153 (2021), 116171.
[17] A.M. Rooney, T.J. McNeill, F.P. Ross, M.P. Bostrom, M.C. van der Meulen, PTH treatment increases cortical bone mass more in response to compression than tension in mice, J. Bone Miner. Res. 38 (2022) 59–69.
[18] T. Sugiyama, L.K. Saxon, G. Zaman, A. Moustafa, A. Sunters, J.S. Price, L. E. Lanyon, Mechanical loading enhances the anabolic effects of intermittent parathyroid hormone (1–34) on trabecular and cortical bone in mice, Bone 43 (2008) 238–248.
[19] C.H. Turner, Three rules for bone adaptation to mechanical stimuli, Bone 23 (1998) 399–407.
[20] J. Wolff, Das gesetz der transformation der knochen, DMW-Deutsche Medizinische Wochenschrift 19 (1893) 1222–1224.
[21] S. Monzem, D. Valkani, L.A.E. Evans, Y.M. Chang, A.A. Pitsillides, Regional modular responses in different bone compartments to the anabolic effect of pth (1-34) and axial loading in mice, Bone 116720 (2023).
[22] B.C. Roberts, H.M. Arredondo Carrera, S. Zanjani-Pour, M. Boudiffa, N. Wang, A. Gartland, E. Dall'Ara, Pth (1–34) treatment and/or mechanical loading have different osteogenic effects on the trabecular and cortical bone in the ovariectomized c57bl/6 mouse, Sci. Rep. 10 (2020) 1–16.
[23] V.S. Cheong, B.C. Roberts, V. Kadirkamanathan, E. Dall'Ara, Positive interactions of mechanical loading and pth treatments on spatiotemporal bone remodelling, Acta Biomater. 136 (2021) 291–305.
[24] B. Javaheri, H. Razi, S. Gohin, S. Wylie, Y.M. Chang, P. Salmon, P.D. Lee, A. A. Pitsillides, Lasting organ-level bone Mechanoadaptation is unrelated to local strain, Sci. Adv. 6 (2020), eaax8301.
[25] C.J. Miller, S. Trichilo, E. Pickering, S. Martelli, P. Delisser, L.B. Meakin, P. Pivonka, Cortical thickness adaptive response to mechanical loading depends on periosteal position and varies linearly with loading magnitude, Front. Bioeng. Biotechnol. 9 (2021) 504.
[26] A.F. Pereira, B. Javaheri, A. Pitsillides, S. Shefelbine, Predicting cortical bone adaptation to axial loading in the mouse tibia, J. R. Soc. Interface 12 (2015), 20150590.
[27] M. Ashrafi, J.E. Gubaua, J.T. Pereira, F. Gahlichi, M. Doblar'e, A mechano-chemo-biological model for bone remodeling with a new mechanochemo- transduction approach, Biomech. Model. Mechanobiol. 19 (2020) 2499–2523.
[28] O.A. Bauchau, J.I. Craig, Structural Analysis, Springer Science & Business Media, 2009.
[29] P.R. Buenzli, C.D.L. Thomas, J.G. Clement, P. Pivonka, Endocortical bone loss in osteoporosis: the role of bone surface availability, Int. J. Num. Methods Biomed. Eng. 29 (2013) 1307–1322.
[30] K.D. Hjelmstad, Fundamentals of Structural Mechanics, 2nd edition, Springer Science & Business Media, 2007.
[31] E. Pickering, S. Trichilo, P. Delisser, P. Pivonka, Beam theory for rapid strain estimation in the mouse tibia compression model, Biomech. Model. Mechanobiol. 21 (2022) 513–525.
[32] S. Trichilo, Assessment of the Anabolic Effects of PTH Drug Treatment and Mechanical Loading on Bone Using High-resolution Imaging and In Silico Modelling, Ph.D. thesis. Ph. D. thesis., University of Melbourne, Melbourne VIC, 2018.
[33] E. Pickering, M.J. Silva, P. Delisser, M.D. Brodt, Y. Gu, P. Pivonka, Estimation of load conditions and strain distribution for in vivo murine tibia compression loading using experimentally informed finite element models, J. Biomech. 115 (2021), 110140.
[34] S. Kohles, J. Bowers, A. Vailas, R. Vanderby Jr., Ultrasonic wave velocity measurement in small polymeric and cortical bone specimens, J. Biomech. Eng. 119 (1997) 232–236.
[35] C.A. Frolik, E.C. Black, R.L. Cain, J.H. Satterwhite, P.L. Brown-Augsburger, M. Sato, J.M. Hock, Anabolic and catabolic bone effects of human parathyroid hormone (1-34) are predicted by duration of hormone exposure, Bone 33 (2003) 372–379.
[36] L.J. Raggatt, N.C. Partridge, Cellular and molecular mechanisms of bone remodeling, J. Biol. Chem. 285 (2010) 25103–25108.
[37] N.A. Sims, T.J. Martin, Coupling the activities of bone formation and resorption: a multitude of signals within the basic multicellular unit, BoneKey Rep. 3 (2014).
[38] I. Matic, B.G. Matthews, X. Wang, N.A. Dyment, D.L. Worthley, D.W. Rowe, D. Grcevic, I. Kalajzic, Quiescent bone lining cells are a major source of osteoblasts during adulthood, Stem Cells 34 (2016) 2930–2942.
[39] M.N. Wein, Bone lining cells: normal physiology and role in response to anabolic osteoporosis treatments, Curr. Molec. Biol. Rep. 3 (2017) 79–84.
[40] C.J. Miller, E. Pickering, S. Martelli, E. Dall'Ara, P. Delisser, P. Pivonka, Cortical bone adaptation response is region specific, but not peak load dependent: insights from μCT image analysis and mechanostat simulations of the mouse tibia loading model, Biomech. Model. Mechanobiol. (2023) 1–18, https://doi.org/10.1007/s10237-023-01775-6.
[41] K.D. Ryder, R. Duncan, Parathyroid hormone modulates the response of osteoblast-like cells to mechanical stimulation, Calcif. Tissue Int. 67 (2000) 241–246.
[42] T.M. Skerry, One mechanostat or many? modifications of the sitespecific response of bone to mechanical loading by nature and nurture, J. Musculoskelet. Neuronal Interact. 6 (2006) 122.
[43] T.M. Skerry, Mechanostat function during skeletal development, J. Musculoskelet. Neuronal Interact. 8 (2008) 12.
[44] H. Yang, W.A. Bullock, A. Myhal, P. DeShield, D. Duffy, R.P. Main, Cancellous bone may have a greater adaptive strain threshold than cortical bone, JBMR Plus 5 (2021), e10489.
[45] C. Hernandez, R. Majeska, M. Schaffler, Osteocyte density in woven bone, Bone 35 (2004) 1095–1099.
[46] F. Shapiro, J.Y. Wu, Woven bone overview: structural classification based on its integral role in developmental, repair and pathological bone formation throughout vertebrate groups, Eur. Cells Mater. 38 (2019) 137–167.
[47] G.L. Galea, L.E. Lanyon, J.S. Price, Sclerostin's role in bone's adaptive response to mechanical loading, Bone 96 (2017) 38–44.
[48] A. Moustafa, T. Sugiyama, J. Prasad, G. Zaman, T.S. Gross, L.E. Lanyon, J.S. Price, Mechanical loading-related changes in osteocyte sclerostin expression in mice are more closely associated with the subsequent osteogenic response than the peak strains engendered, Osteoporos. Int. 23 (2012) 1225–1234.
[49] A.G. Robling, P.J. Niziolek, L.A. Baldridge, K.W. Condon, M.R. Allen, I. Alam, S. M. Mantila, J. Gluhak-Heinrich, T.M. Bellido, S.E. Harris, C.H. Turner, Mechanical stimulation of bone in vivo reduces osteocyte expression of Sost/sclerostin, J. Biol. Chem. 283 (9) (2008) 5866–5875.
[50] T. Sugiyama, L.B. Meakin, W.J. Browne, G.L. Galea, J.S. Price, L.E. Lanyon, Bones' adaptive response to mechanical loading is essentially linear between the low strains associated with disuse and the high strains associated with the lamellar/woven bone transition, J. Bone Miner. Res. 27 (2012) 1784–1793.